instruments

MDPI

Article

Polyethylene Identification in Ocean Water Samples by Means of 50 keV Energy Electron Beam

John I. Adlish [1,2], Davide Costa [2], Enrico Mainardi [2], Piero Neuhold [2,*], Riccardo Surrente [2] and Luca J. Tagliapietra [2,*]

[1] Biology Department, Truckee Meadow Community College, Reno, Nevada, NV 89512-3999, USA; john.adlish@babuhawaiifoundation.org

[2] Particle Physics Department, BabuHawaii Foundation, Honolulu, HI 96811, USA; davide@babuhawaiifoundation.org (D.C.); enrico.mainardi@babuhawaiifoundation.org (E.M.); rick@babuhawaiifoundation.org (R.S.)

* Correspondence: piero@babuhawaiifoundation.org (P.N.); lucaj@babuhawaiifoundation.org (L.J.T.)

Received: 16 September 2020; Accepted: 21 October 2020; Published: 31 October 2020

Abstract: This study presents a new methodology to reveal traces of polyethylene (the most common microplastic particles, known as a structure of C_2H_4) in a sample of ocean water by the irradiation of a 50 keV, 1 μA electron beam. This is performed by analyzing the photon (produced by the electrons in water) fluxes and spectra (i.e., fluxes as a function of photon energy) with different types of contaminated water using an adequate device and in particular looking at the peculiar interactions of electrons/photons with the potential abnormal atomic hydrogen (H), oxygen (O), carbon (C), and phosphorus (P) compositions present in the water, as a function of living and nonliving organic organisms with PO_4 group RNA/DNA strands in a cluster configuration through a volumetric cells grid.

Keywords: microplastics; polyethylene ocean water; microplastics identification; microorganisms identification; ocean water quality; drinking water; food quality; cancer and microplastics; plastic and ocean; particle physics; particle accelerators in environmental studies

1. Introduction

Plastic is the most common type of marine debris found in oceans, and it is the most widespread problem affecting the marine environment. It also threatens ocean health, food safety and quality, human health, and coastal tourism, and it contributes to climate change [1–5]. Plastic debris can come in many different shapes and sizes, but those that are less than five millimeters across (or the size of a sesame seed) are called "microplastics". One of the most common microplastics in use today is polyethylene, with most of the known kinds having the chemical formula $(C_2H_4)_n$. It is a linear, man-made homopolymer primarily used for packaging (plastic bags, plastic films, geomembranes, containers including bottles, etc.). As of 2019, over 100 million tons of polyethylene resins are being produced annually, accounting for 34% of the total plastics market.

This is an emerging field of study, and not much is known yet about microplastics and their impact on the environment. The NOAA Marine Debris Program is pursuing efforts within the NOAA to research this important topic.

Different standardized field methods have been developed for the collection of microplastic samples in sediment [6–13], sand, and surface water, all of which continue to be tested. In the end, the field and laboratory protocols will allow for a global comparison of the quantity of microplastics released into the environment, which is the first step in determining the final distribution, impacts, and fate of these debris.

Microplastics come from a variety of sources, including larger plastic debris that degrade into smaller and smaller pieces. In addition, microspheres, a type of microplastic, are tiny particle pieces of plastic polyethylene that are added as exfoliators to health and beauty products, such as some detergents and toothpastes, passing easily through water filtration systems, thus posing a threat to aquatic life.

The most visible impacts of marine plastics are the ingestion, suffocation, and entanglement of hundreds of marine species. Marine wildlife such as seabirds, whales, fish, and turtles, mistake plastic waste for prey, and most die of starvation as their stomachs are filled with plastic debris. They also suffer from lacerations, infections, reduced ability to swim, and internal injuries. Floating plastics also contribute to the spread of invasive marine organisms and bacteria, which disrupt ecosystems. Plastic degrades (i.e., breaks down into pieces), but it does not biodegrade (break down through natural decomposition). This has become a problem over time, as all the plastic pieces that have been generated over the last seven decades have steadily increased their presence as a contaminant, creating a biological alteration. According to the United Nations Environment Program, these plastic microspheres first appeared in personal care products about fifty years ago, with plastic replacing more and more natural ingredients. Until 2012, this problem was still relatively unknown, with an abundance of products containing plastic microspheres on the market and leading now to an increase in microplastic detection and identification demand.

Ocean water also contains microorganisms, live matter and not, such as viruses, bacteria, and microorganisms like plankton with a different PO_4 phosphorus content [14–29]. Viruses, for example, are intracellular parasites composed of a nucleic acid surrounded by a protein coat, the capsid. Some viruses contain a lipid envelope, derived from the host, surrounding the capsid. The nucleic acid found in viruses can consist of either RNA or DNA. RNA is composed of nucleotides, each containing a sugar (deoxyribose), a nitrogen-containing base (adenine, uracil, guanine, and cytosine), and a phosphate group PO_4. Members of the Coronoviridae family measure 80–160 nm in diameter. Generally, there are 1–10 million viruses and about 100,000 to 1 million bacteria cells for each milliliter of ocean water.

The proposed methodology is based on a subatomic particle analysis and the subsequent detection of particles, and the aim is to use this to identify polyethylene particles in the water among microorganisms. It could be an interesting research approach for the ocean studies field and for the food and beverage industries field in order to detect microplastic contamination in their products. This type of approach would make it easier to test water samples and analyze data in real time in comparison to other state-of-the-art detection processes, and it also allows test procedures to be conducted for quality assurance in the food and beverage industries with simple hardware.

2. Materials and Methods

The physical model under analysis and its simulation by the MCNPX Monte Carlo simulation subatomic particles code [30–32] are based on an electron beam source of 50 keV and 1 μA, easily accessible from an extraction line of an industrial linear/circular particle accelerator, interacting with the water sample target. The beam energy and current are based on cross section considerations and radiation requirements; the beam interacts with a cylindrical sample volume—with the axis on x—of ocean water of radius r = 5 cm and height h = 10 cm as *s* sample tank (Figure 1), which is analyzed at x = 10 cm through a double plates ionization chamber detector.

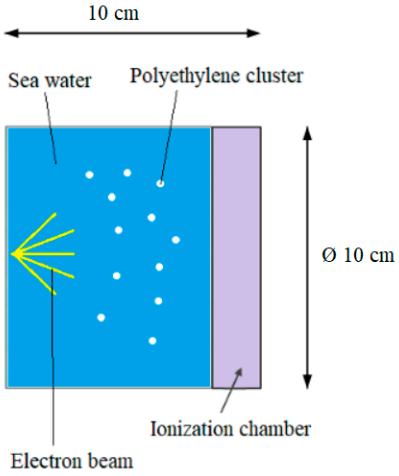

Figure 1. Physical model x-z section of ocean water and polyethylene.

The ocean water taken into account was chemically analyzed, as shown in Table 1 [12].

Table 1. Ocean water weight chemical composition.

Element.	Element (%)	Element	Element (%)
Oxygen	85.7	Molybdenum	0.000001
Hydrogen	10.8	Zinc	0.000001
Chlorine	1.9	Nickel	0.00000054
Sodium	1.05	Arsenic	0.0000003
Magnesium	0.135	Copper	0.0000003
Sulfur	0.0885	Tin	0.0000003
Calcium	0.04	Uranium	0.0000003
Potassium	0.038	Chromium	0.00000003
Bromine	0.0065	Krypton	0.00000025
Carbon	0.0028	Manganese	0.0000002
Strontium	0.00081	Vanadium	0.0000001
Boron	0.00046	Titanium	0.0000001
Silicon	0.0003	Cesium	0.00000005
Fluoride	0.00013	Cerium	0.00000004
Argon	0.00006	Antimony	0.000000033
Nitrogen	0.00005	Silver	0.00000003
Lithium	0.000018	Yttrium	0.00000003
Rubidium	0.000012	Cobalt	0.000000027
Phosphorus	0.000007	Neon	0.000000014
Iodine	0.000006	Cadmium	0.000000011
Barium	0.000003	Tungsten	0.00000001
Aluminum	0.000001	Lead	0.000000005
Iron	0.000001	Mercury	0.000000003
Indium	0.000001	Selenium	0.000000002

Among the all possible subatomic particles generated, only photons (coming from electron coherent and incoherent scattering, absorption, knock on, decay, fluorescence, bremsstrahlung, and photoelectric effect) were taken into account, as reported in Table 2 (where the percent contribution of different phenomena which create photons are shown) and Table 3 (where the percent contribution of different elements to the production of photons are shown), as the other ones are actually negligible. As for Table 2, the photoelectric effect consists of the absorption of the incident photon energy E, with emission of several fluorescent photons and the ejection or excitation of an orbital electron of binding energy $e < E$. Photons of first fluorescence are emitted with energy greater than 1 keV; those of second fluorescence are still greater than 1 keV and are caused by residual excitation of the first fluorescence process, leading to a second emission.

It has to be underlined that the MCNPX analysis took into account both electrons and photons without neglecting any secondary photon production by performing a photon/electron coupled calculation and by keeping track of the electron mean free path in the water sample, which is around 5060 nm due to multiple volume cells of the electron mean path magnitude. All the results proposed concern the photon fluxes and spectra of interest, where all the possible primary and secondary electron productions (mode e, p) into the sample volume were taken into account.

Table 2. Photon Creation.

	Ocean Water No Contamination	Polyethylene 10 ppm	Polyethylene 100 ppm	Polyethylene 1000 ppm	Polyethylene 10,000 ppm
Bremsstrahlung	99.1265%	99.1237%	99.1182%	99.1545%	99.3538%
1st Fluorescence	0.8733%	0.8755%	0.8812%	0.8449%	0.6448%
2nd Fluorescence	0.0002%	0.0008%	0.0006%	0.0006%	0.0015%
Norm	100.0000%	100.0000%	100.0000%	100.0000%	100.0000%

Table 3. Nuclide Photon Activity.

Element	Ocean Water No Contamination	Polyethylene 10 ppm	Polyethylene 100 ppm	Polyethylene 1000 ppm	Polyethylene 10,000 ppm
Oxygen	76.210%	76.273%	76.387%	73.211%	52.813%
Hydrogen	7.585%	7.405%	6.998%	6.686%	4.259%
Chlorine	12.357%	12.107%	12.179%	11.938%	8.902%
Sodium	1.924%	1.912%	1.873%	1.912%	1.384%
Magnesium	0.306%	0.325%	0.316%	0.370%	0.244%
Sulfur	0.490%	0.573%	0.536%	0.448%	0.372%
Calcium	0.429%	0.512%	0.434%	0.409%	0.277%
Potassium	0.316%	0.360%	0.337%	0.384%	0.330%
Bromine	0.322%	0.294%	0.281%	0.340%	0.198%
Carbon	0.000%	0.193%	0.628%	4.257%	31.188%
Strontium	0.056%	0.046%	0.031%	0.044%	0.029%
Silicon	0.005%	0.000%	0.000%	0.000%	0.000%
Argon	0.000%	0.000%	0.000%	0.000%	0.004%

The polyethylene particles are described in 11 cluster configurations (Table 4) through a highly sophisticated volumetric cell grid (Figures 2 and 3); each cluster is composed of microspheres with a radius of 0.1 mm and a volume of $4 \times 10^{19} - 3$ mm^3 per particle, with a mutual distance of 1–9 cm among the clusters along all the axes (Figure 3) and evaluated on an atomic fraction of C, H in the ocean water sample tank at different concentrations from 10 ppm up to 10,000 ppm (Tables 5–8).

Table 4. Parts per million contamination in cluster configuration.

Cluster N	(10 ppm)	(100 ppm)	(1000 ppm)	(10,000 ppm)
	ppm perCluster	*ppm perCluster*	*ppm perCluster*	*ppm perCluster*
1	1	10	100	1000
2	0.5	5	50	500
3	2	20	200	2000
4	1.3	13	130	1300
5	1.9	19	190	1900
6	0.3	3	30	300
7	0.8	8	80	800
8	0.4	4	40	400
9	0.2	2	20	200
10	0.9	9	90	900
11	0.7	7	70	700
Norm	*10*	*100*	*1000*	*10,000*

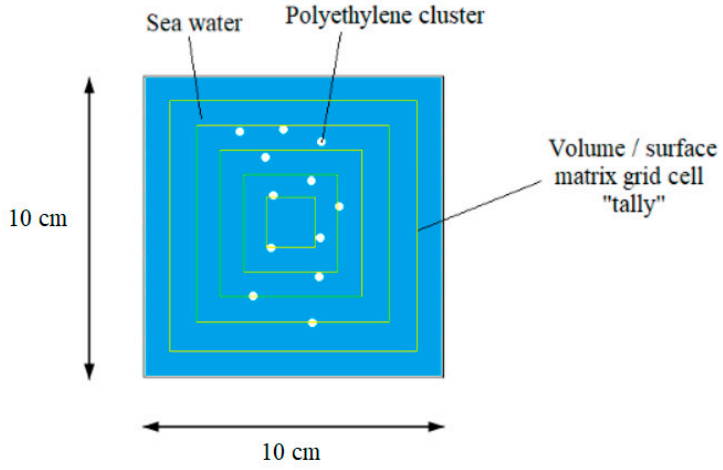

Figure 2. Geometrical model of x-z section.

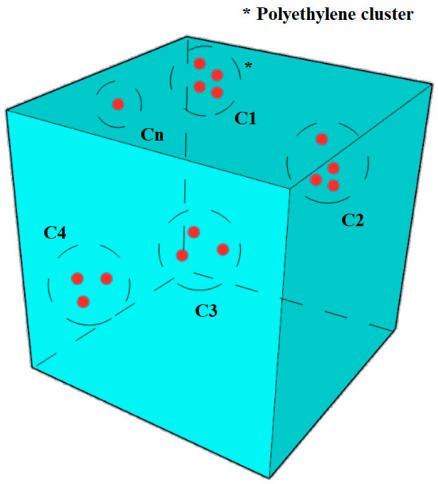

Figure 3. Volumetric cluster cells in 3D.

Table 5. Particles and volume in 10 ppm.

Cluster N	(10 ppm)	(10 ppm)	Particles N	Volume (mm^3)
	ppm per Cluster	*% ppm Cluster*	*per Cluster*	*per Cluster*
1	1	10%	262	1
2	0.5	5%	131	1
3	2	20%	525	2
4	1.3	13%	341	1
5	1.9	19%	498	2
6	0.3	3%	79	0.3
7	0.8	8%	210	1
8	0.4	4%	105	0.4
9	0.2	2%	52	0.2
10	0.9	9%	236	1
11	0.7	7%	184	1
Norm	10	100.00%	2623	11

Table 6. Particles and volume in 100 ppm.

Cluster N	(100 ppm)	(100 ppm)	Particles N	Volume (mm^3)
	ppm per Cluster	*% ppm Cluster*	*per Cluster*	*per Cluster*
1	10	10%	2623	11
2	5	5%	1311	5
3	20	20%	5245	22
4	13	13%	3409	14
5	19	19%	4983	21
6	3	3%	787	3
7	8	8%	2098	9
8	4	4%	1049	4
9	2	2%	525	2
10	9	9%	2360	10
11	7	7%	1836	8
Norm	100	100.00%	26,227	110

Table 7. Particles and volume in 1000 ppm.

Cluster N	(1000 ppm)	(1000 ppm)	Particles N	Volume (mm^3)
	ppm per Cluster	*% ppm Cluster*	*per Cluster*	*per Cluster*
1	100	10%	26,227	110
2	50	5%	13,113	55
3	200	20%	52,454	220
4	130	13%	34,095	143
5	190	19%	49,831	209
6	30	3%	7868	33
7	80	8%	20,981	88
8	40	4%	10,491	44
9	20	2%	5245	22
10	90	9%	23,604	99
11	70	7%	18,359	77
Norm	1000	100.00%	262,268	1099

Table 8. Particles and volume in 10,000 ppm.

Cluster N	(10,000 ppm)	(10,000 ppm)	Particles N	Volume (mm^3)
	ppm per Cluster	*% ppm Cluster*	*per Cluster*	*per Cluster*
1	1000	10%	262,268	1099
2	500	5%	131,134	549
3	2000	20%	524,535	2198
4	1300	13%	340,948	1429
5	1900	19%	498,308	2088
6	300	3%	78,680	330
7	800	8%	209,814	879
8	400	4%	104,907	440
9	200	2%	52,454	220
10	900	9%	236,041	989
11	700	7%	183,587	769
Norm	10,000	100.00%	2,622,676	10,989

It must be underlined that a benchmark model was also taken into consideration in order to evaluate a potential enrichment in microorganisms, bacteria, and viruses, which can alter mainly the carbonium and in particular the phosphorus PO_4 group analysis outcome; these all were analyzed on multiple "tallies" (control check volumes/surfaces) in order to evaluate energy distributions and particle mean free path (yellow squares, Figure 4). In order to do that, in the benchmark, a 100-ppm polyethylene content in the ocean water sample in the cluster configuration was kept constant, and different enriched mixture scenarios at 0.7 ppm, 7 ppm, 70 ppm, and 700 ppm of potential living/nonliving matter and microorganisms were studied, adjusting their own contributions in the final solution in terms of atomic C, H, O, P content and the result in terms of particle spectra and fluxes.

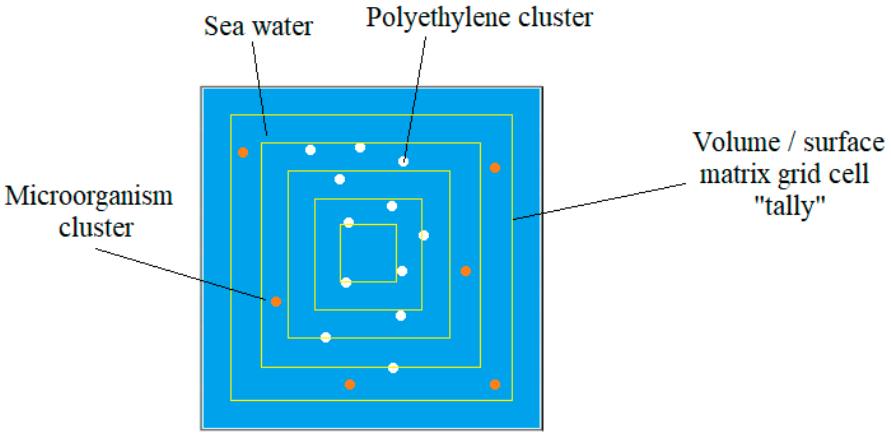

Figure 4. Ocean water polyethylene plus microorganisms, x-z section model.

MCNPX was performed chronologically in different cluster stages: Stage 1, with 0 ppm contamination to investigate the physics involved in the basic case; Stage 2, evaluating an escalating contamination grade as maximum stress test of 10 ppm, 100 ppm, 1000 ppm, and 10,000 ppm (Tables 9 and 10), just as a benchmark to determine the subatomic particles' stopping power and the shielding effects that give the photon fluxes and energy spectra, due to all the experimental cross sections involved in these cases (Figures 5–24). The MCNPX code by various variance reduction techniques fulfils 10 statistical tests [30] with an average relative error of 2%.

Table 9. Polyethylene ppm.

	C	H
ppm	**(mg/L)**	**(mg/L)**
10	8.57142857	1.42857143
100	85.7142857	14.2857143
1000	857.142857	142.857143
10,000	8571.42857	1428.57143

Table 10. Ocean Water Vs Polyethylene ppm composition.

Element	Origin Element (%)	Element (ppm)	10 ppm Polyethylene (ppm)	100 ppm Polyethylene (ppm)	1000 ppm Polyethylene (ppm)	10,000 ppm Polyethylene (ppm)
Oxygen	85.70	8.57×10^5	8.570×10^5	8.569×10^5	8.561×10^5	8.484×10^5
Hydrogen	10.80	1.08×10^5	1.080×10^5	1.080×10^5	1.081×10^5	1.094×10^5
Chlorine	1.90	19,000	1.900×10^4	1.900×10^4	1.898×10^4	1.881×10^4
Sodium	1.05	10,500	1.050×10^4	1.050×10^4	1.049×10^4	1.040×10^4
Magnesium	0.14	1350	1.350×10^3	1.350×10^3	1.349×10^3	1.337×10^3
Sulfur	0.09	885	8.850×10^2	8.849×10^2	8.841×10^2	8.762×10^2
Calcium	0.04	400	4.000×10^2	4.000×10^2	3.996×10^2	3.960×10^2
Potassium	0.04	380	3.800×10^2	3.800×10^2	3.796×10^2	3.762×10^2
Bromine	0.01	65	6.500×10^1	6.499×10^1	6.494×10^1	6.435×10^1
Carbon	0.00	28	3.657×10^1	1.137×10^2	8.851×10^2	8.599×10^3

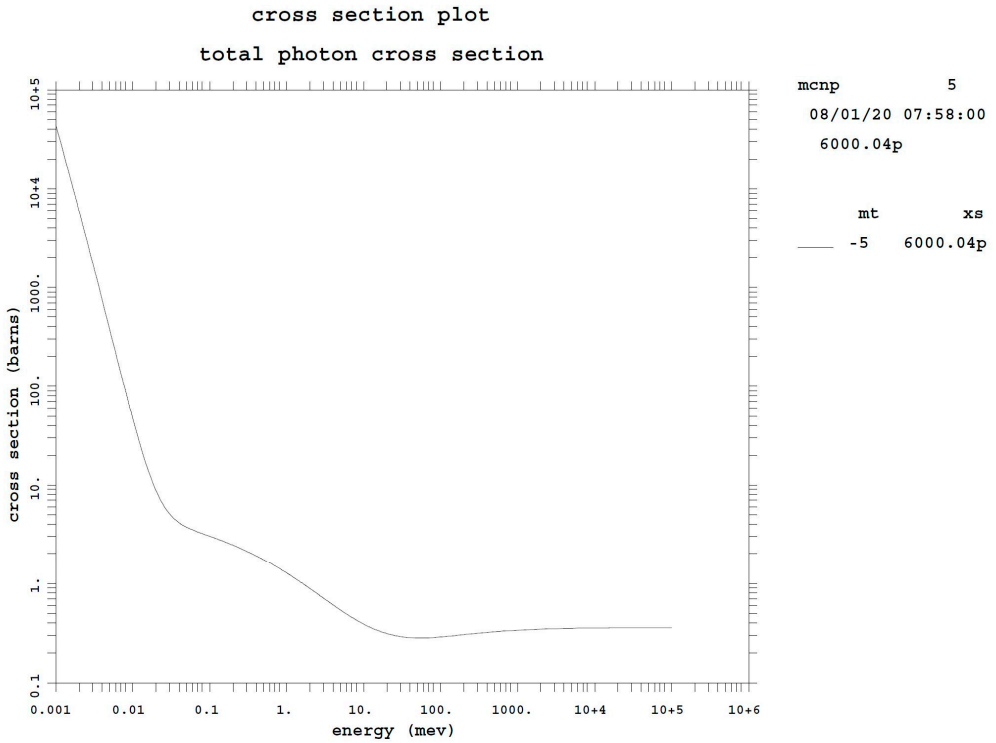

Figure 5. Carbon total photon cross section as a function of energy.

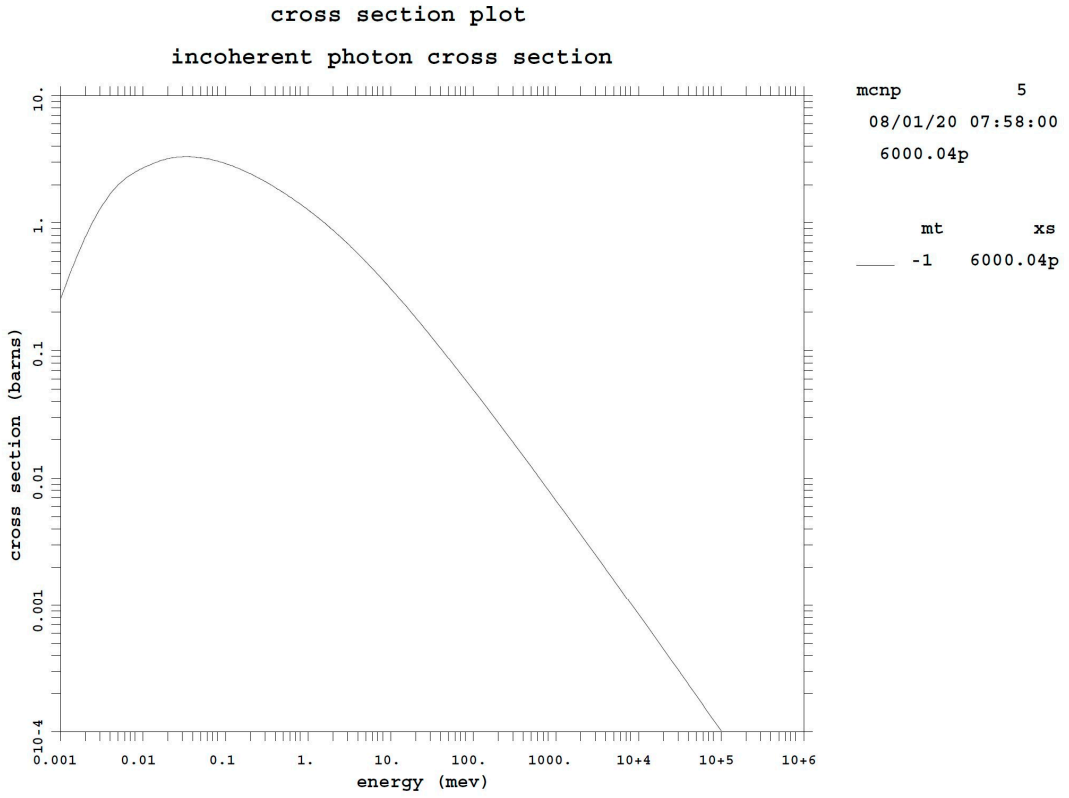

Figure 6. Carbon incoherent photon cross section as a function of energy.

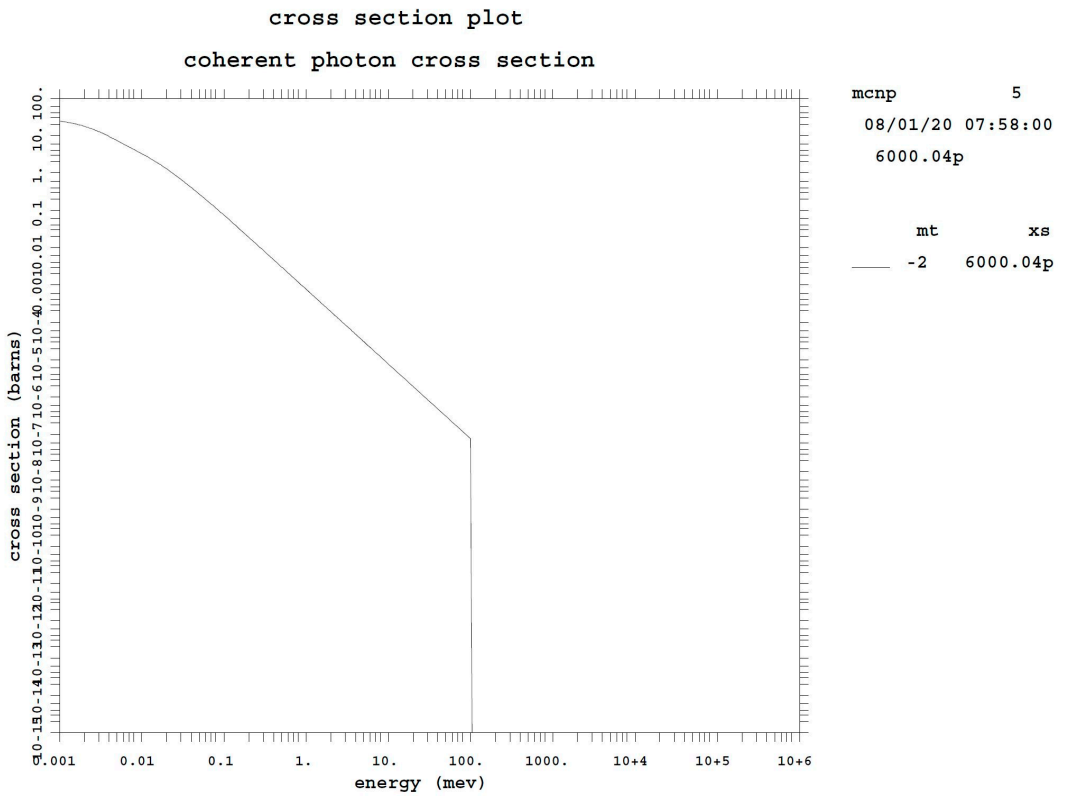

Figure 7. Carbon coherent photon cross section as a function of energy.

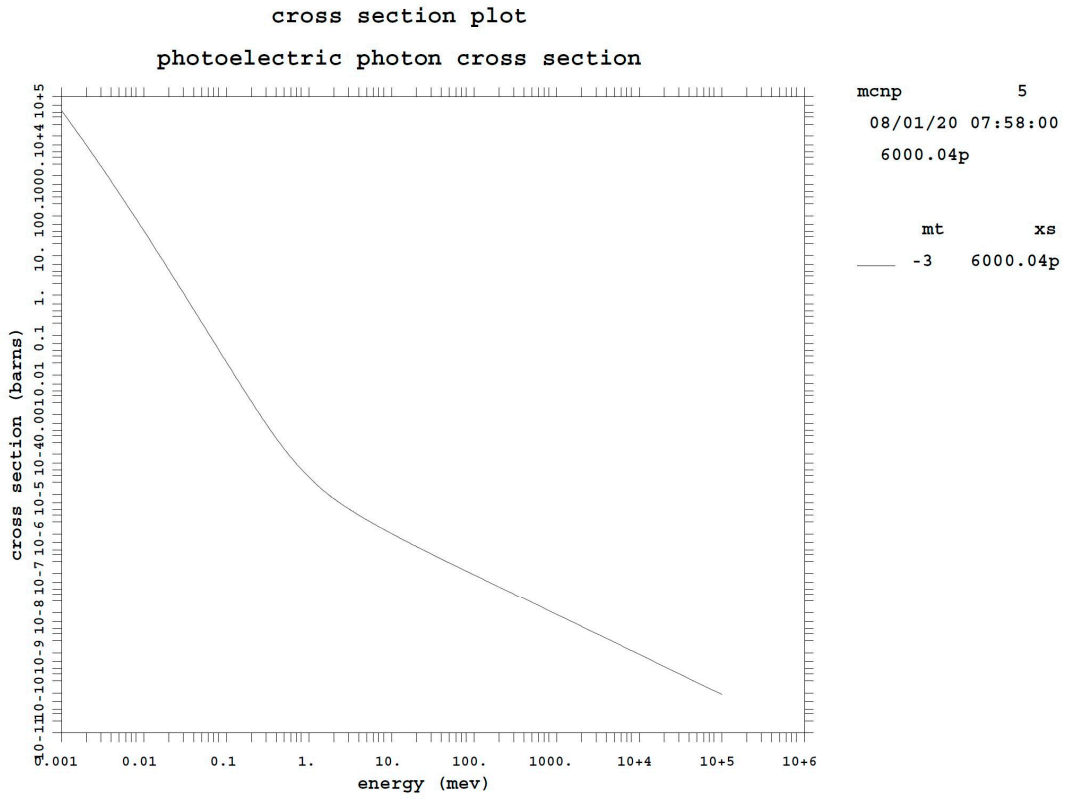

Figure 8. Carbon photoelectric photon cross section as a function of energy.

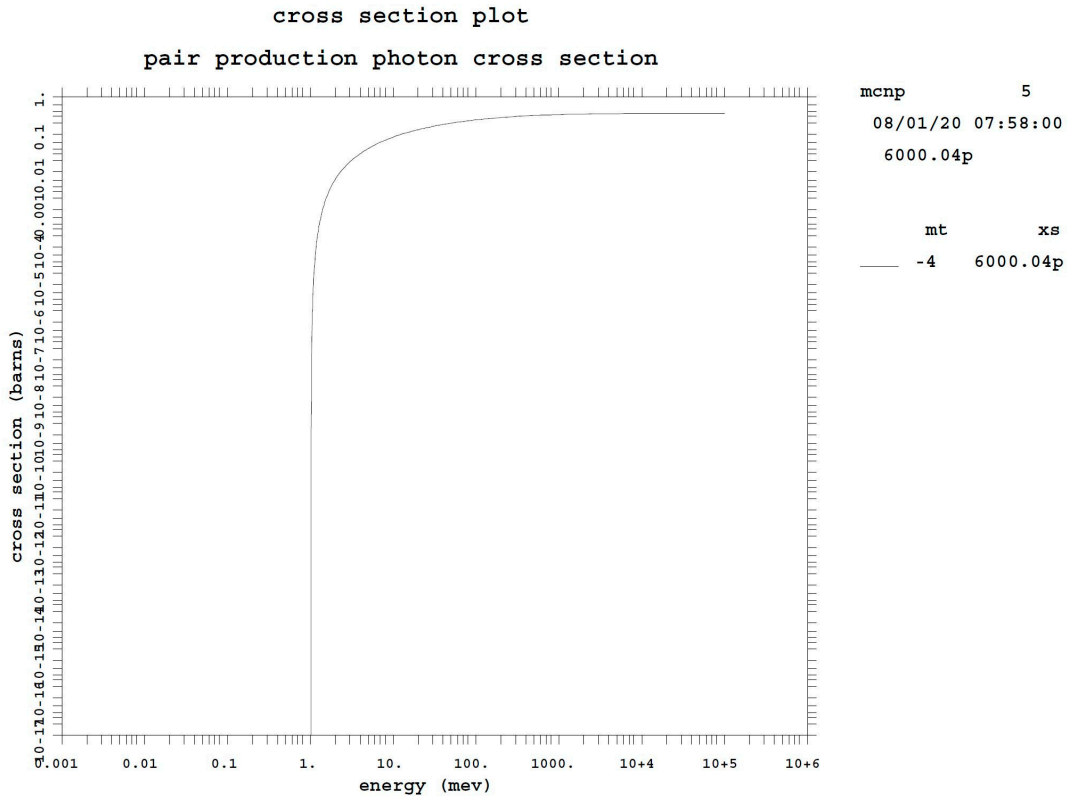

Figure 9. Carbon pair production photon cross section as a function of energy.

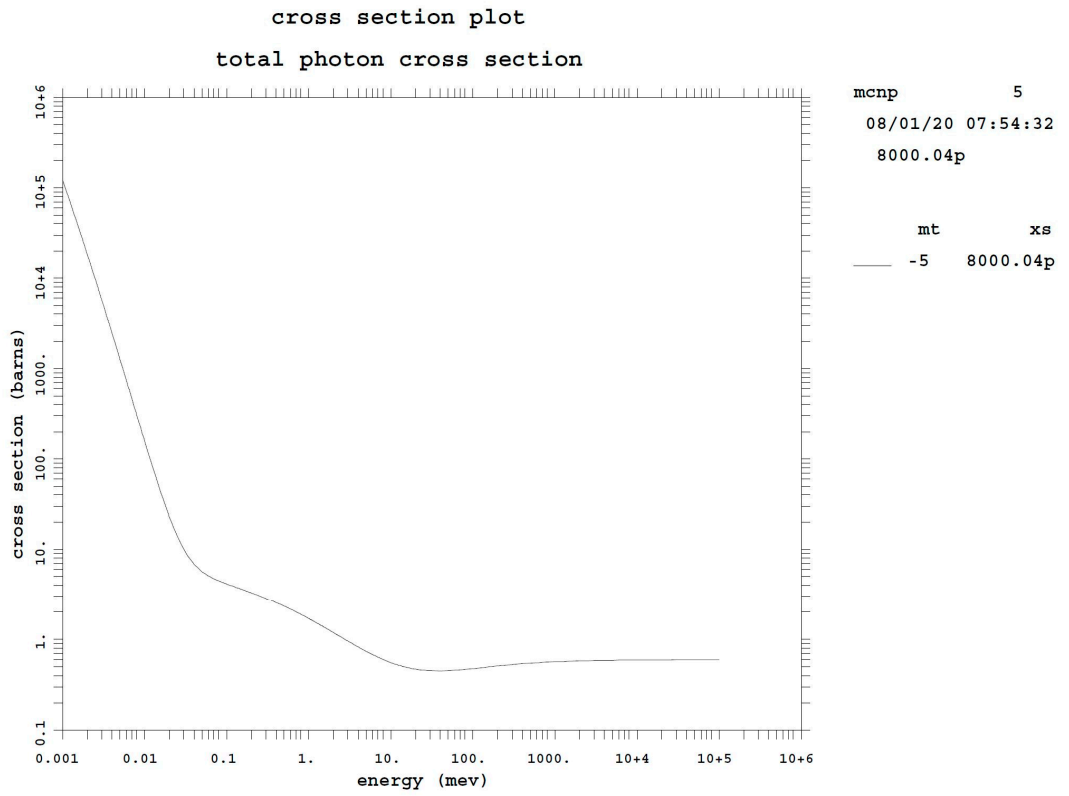

Figure 10. Oxygen total photon cross section as a function of energy.

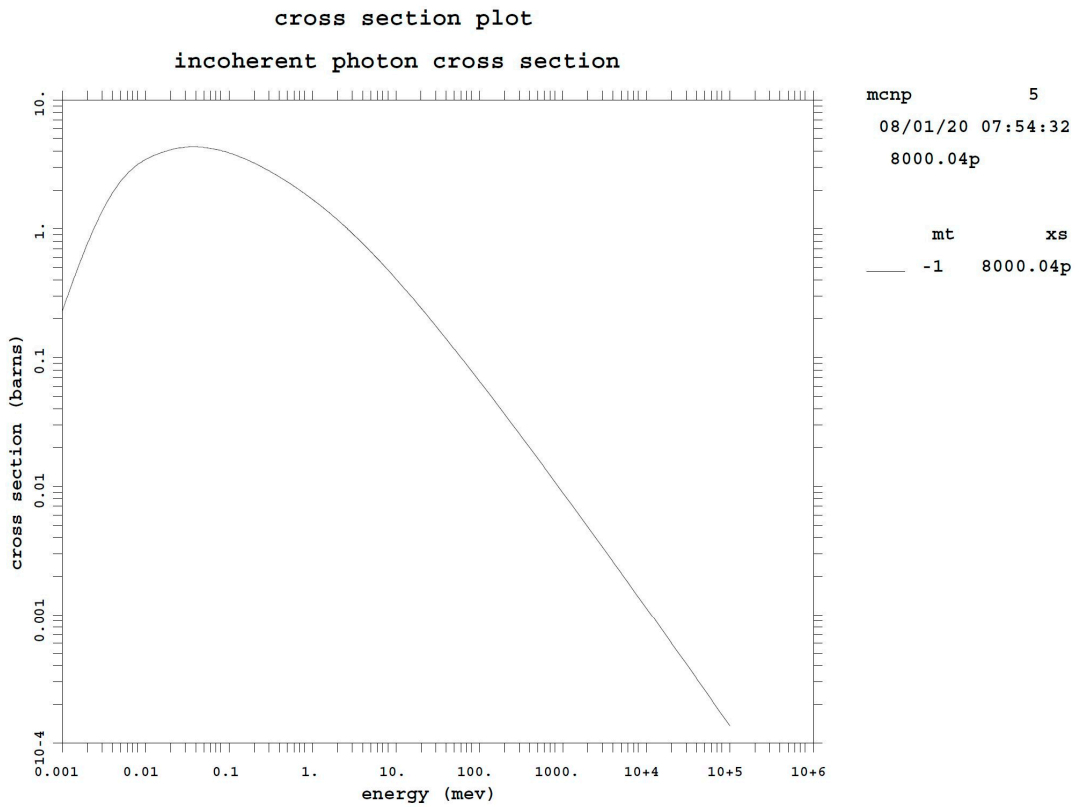

Figure 11. Oxygen incoherent photon cross section as a function of energy.

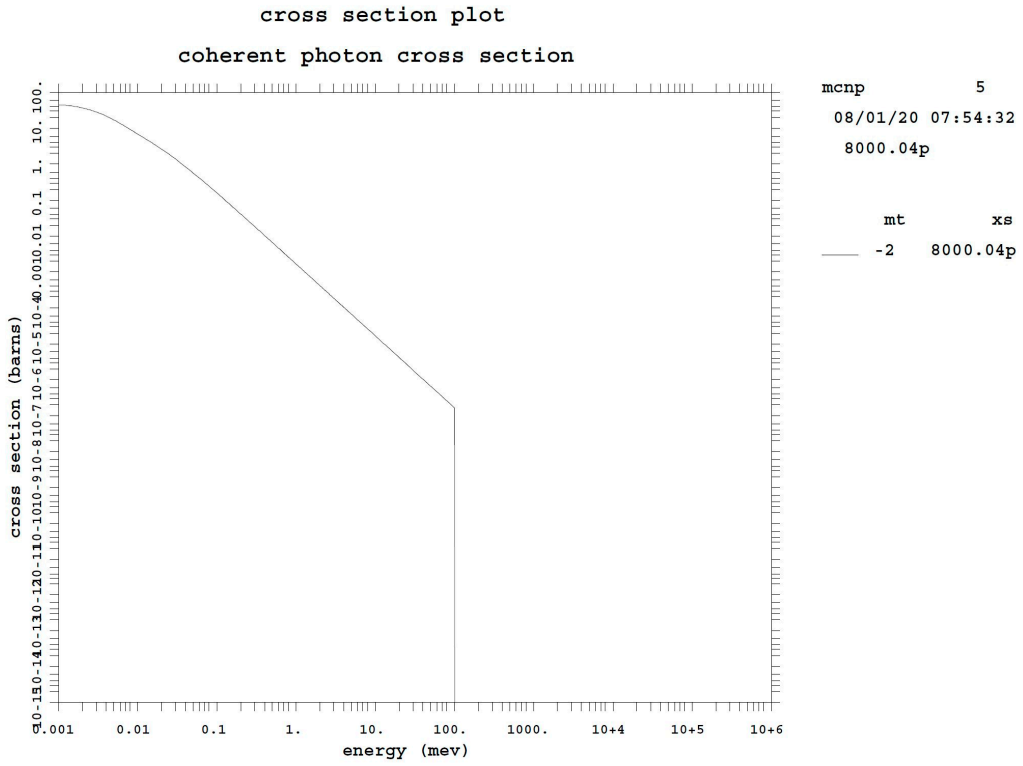

Figure 12. Oxygen coherent photon cross section as a function of energy.

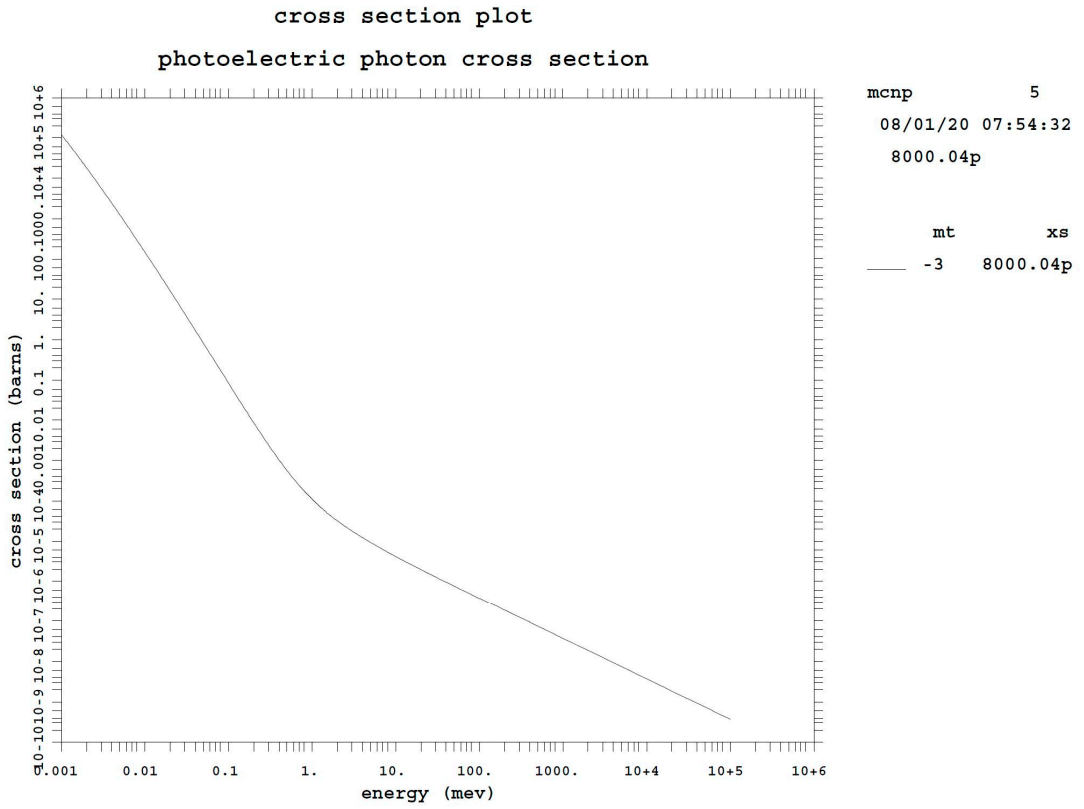

Figure 13. Oxygen photoelectric photon cross section as a function of energy.

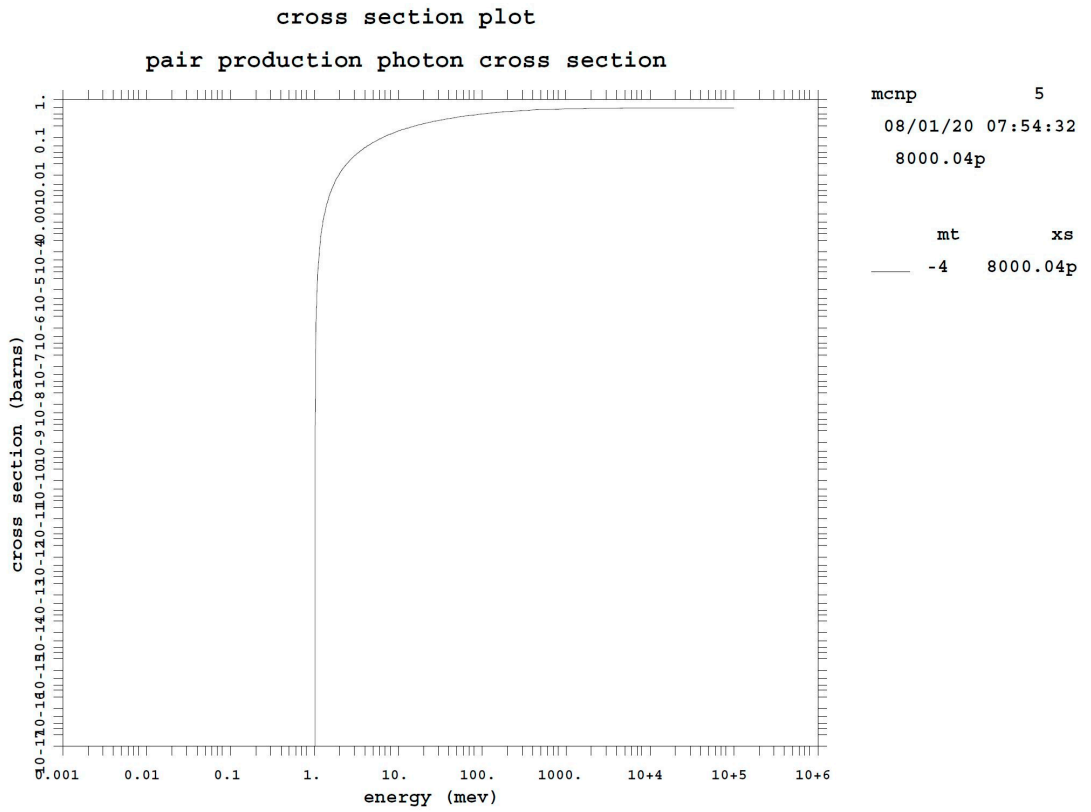

Figure 14. Oxygen pair production photon cross section as a function of energy.

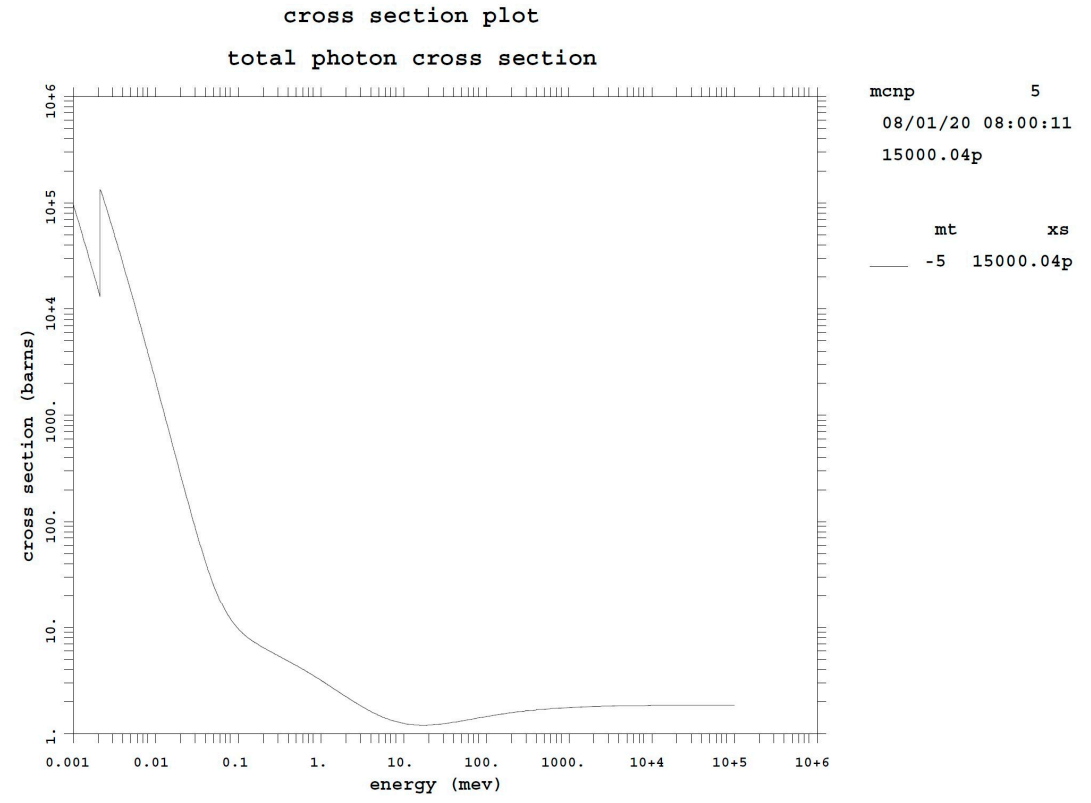

Figure 15. Phosphorus total photon cross section as a function of energy.

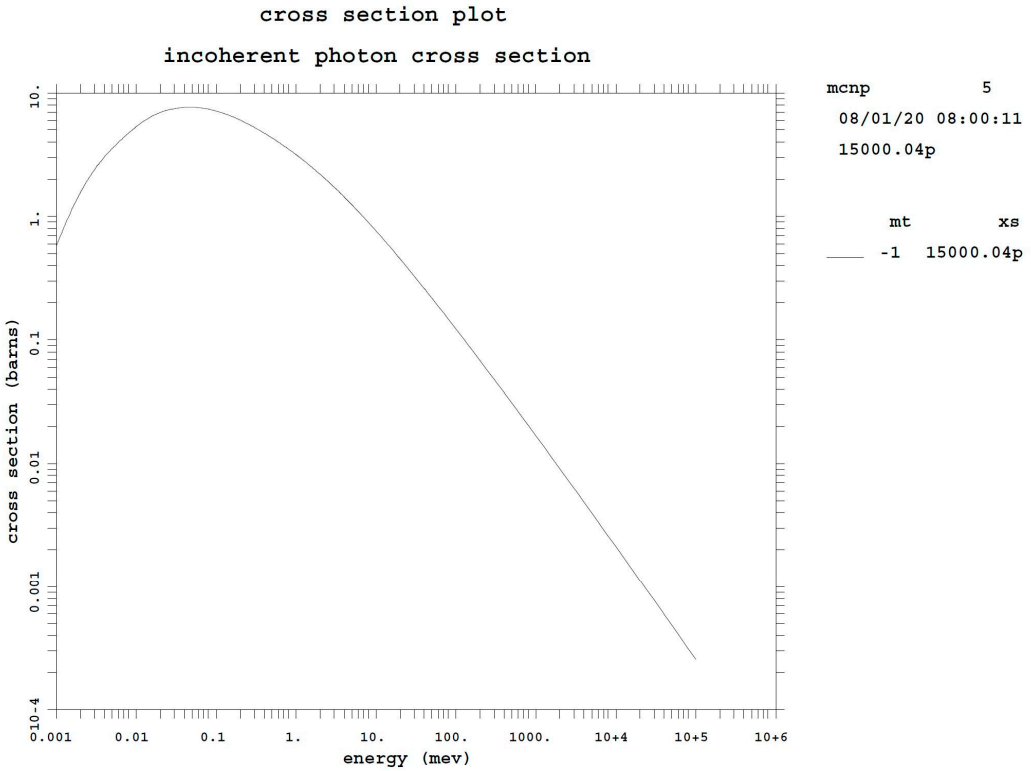

Figure 16. Phosphorus incoherent photon cross section as a function of energy.

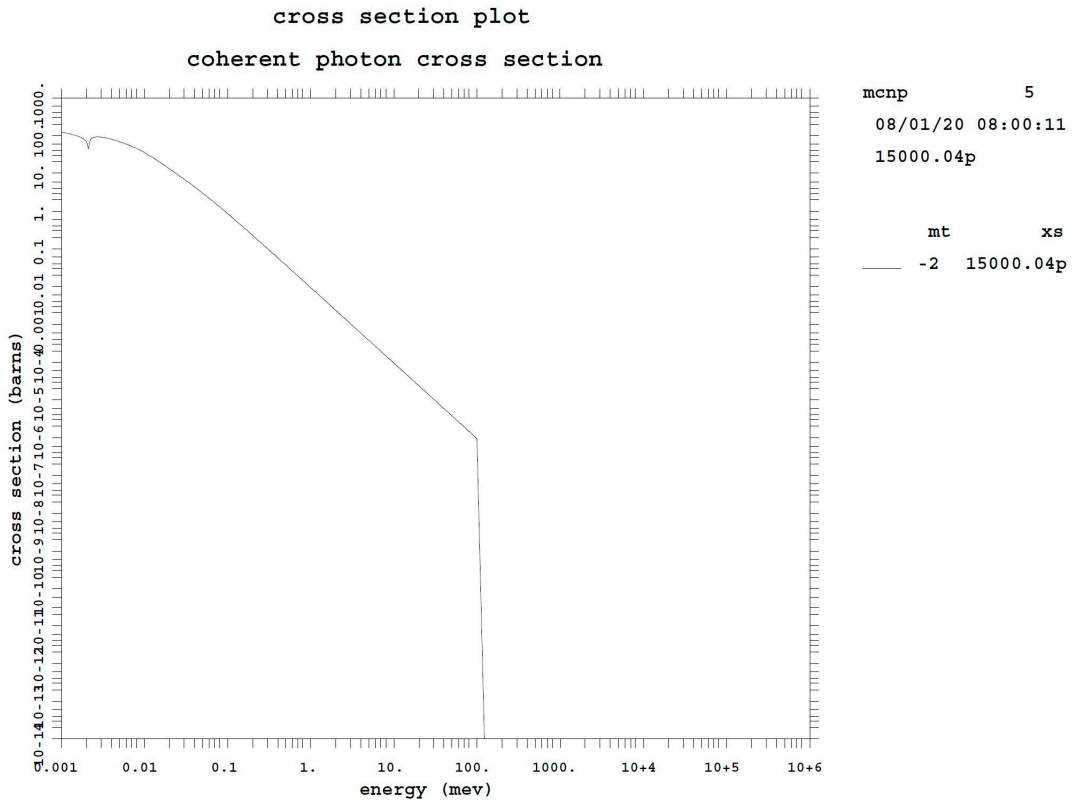

Figure 17. Phosphorus coherent photon cross section as a function of energy.

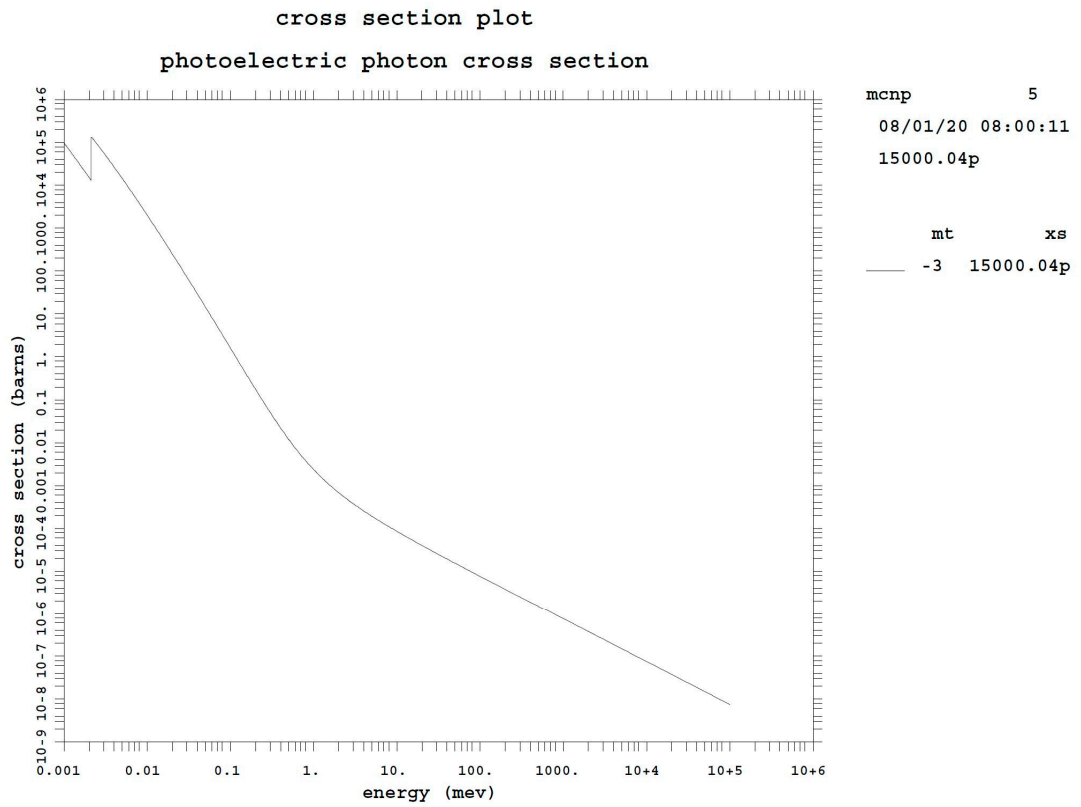

Figure 18. Phosphorus photoelectric photon cross section as a function of energy.

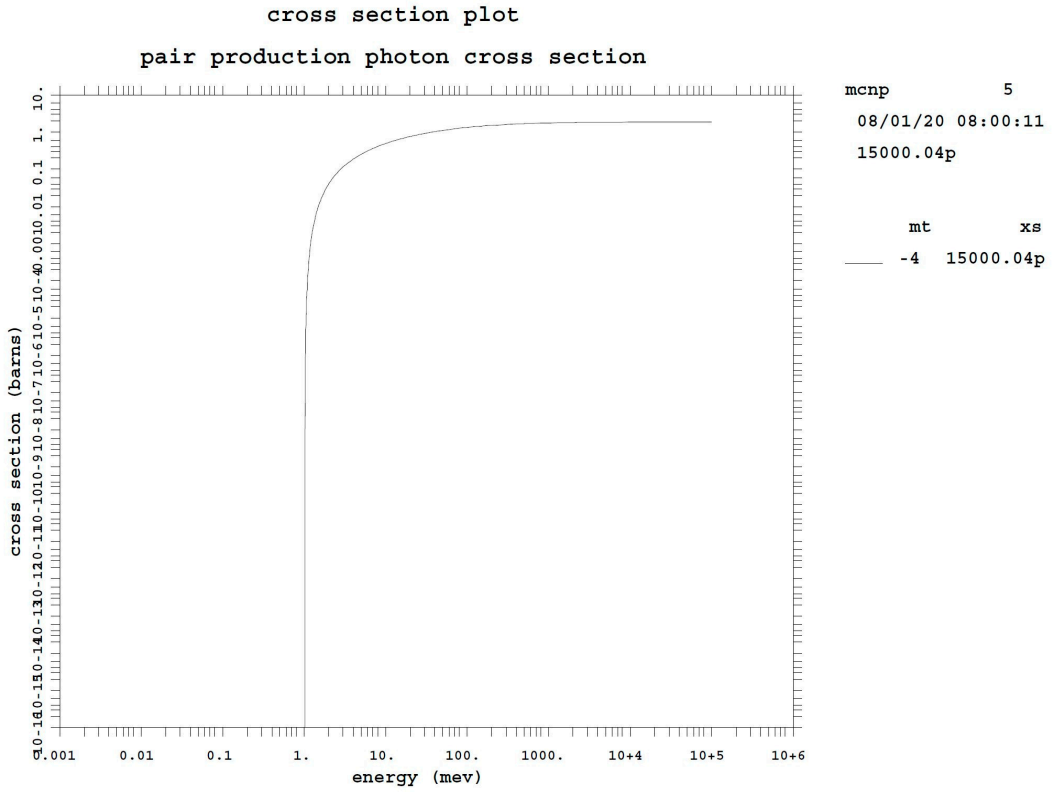

Figure 19. Phosphorus pair production photon cross section as a function of energy.

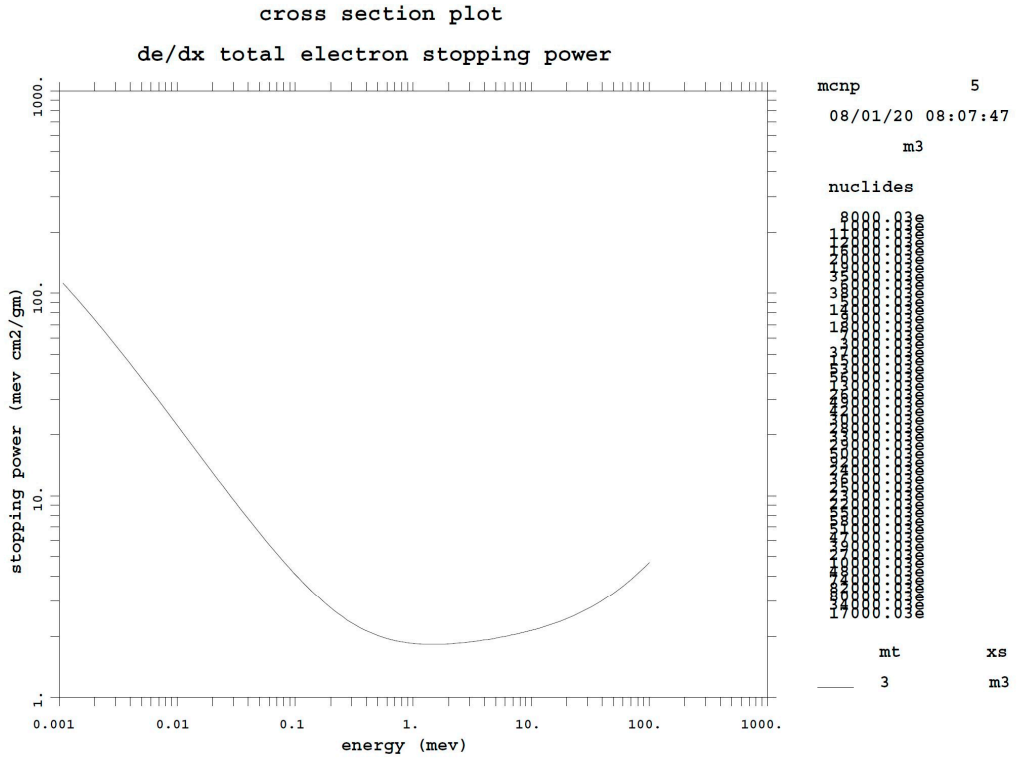

Figure 20. Ocean water total electron stopping power as a function of energy.

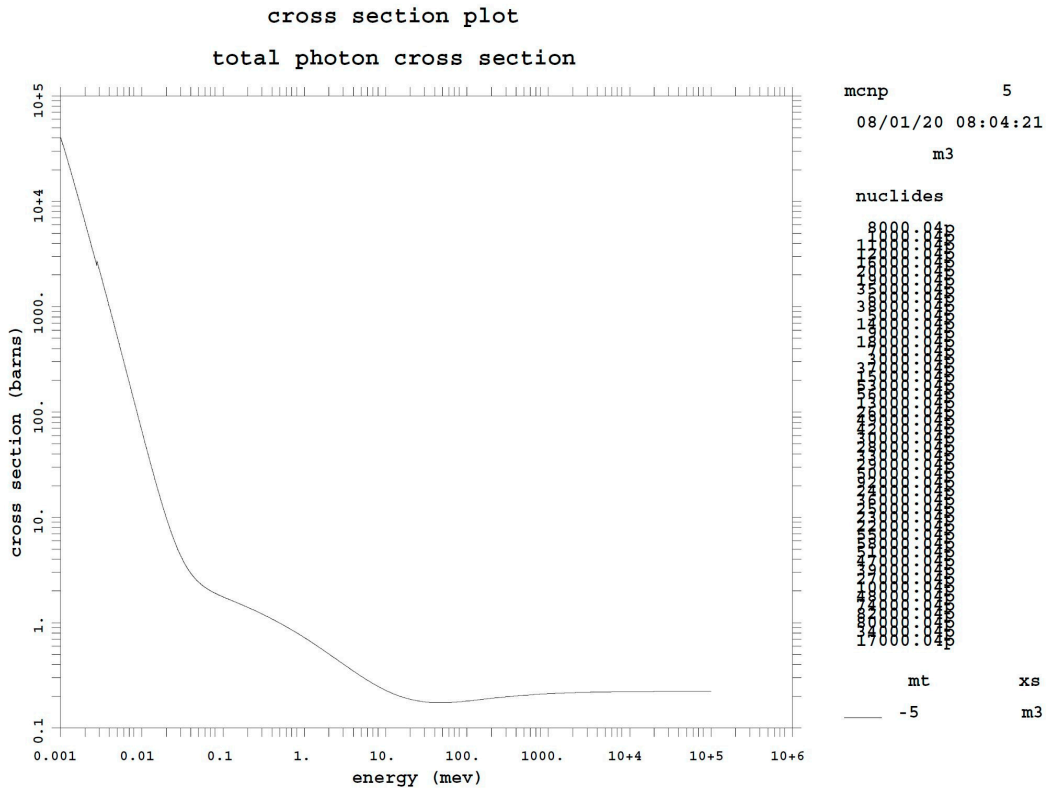

Figure 21. Ocean water total photon cross section as a function of energy.

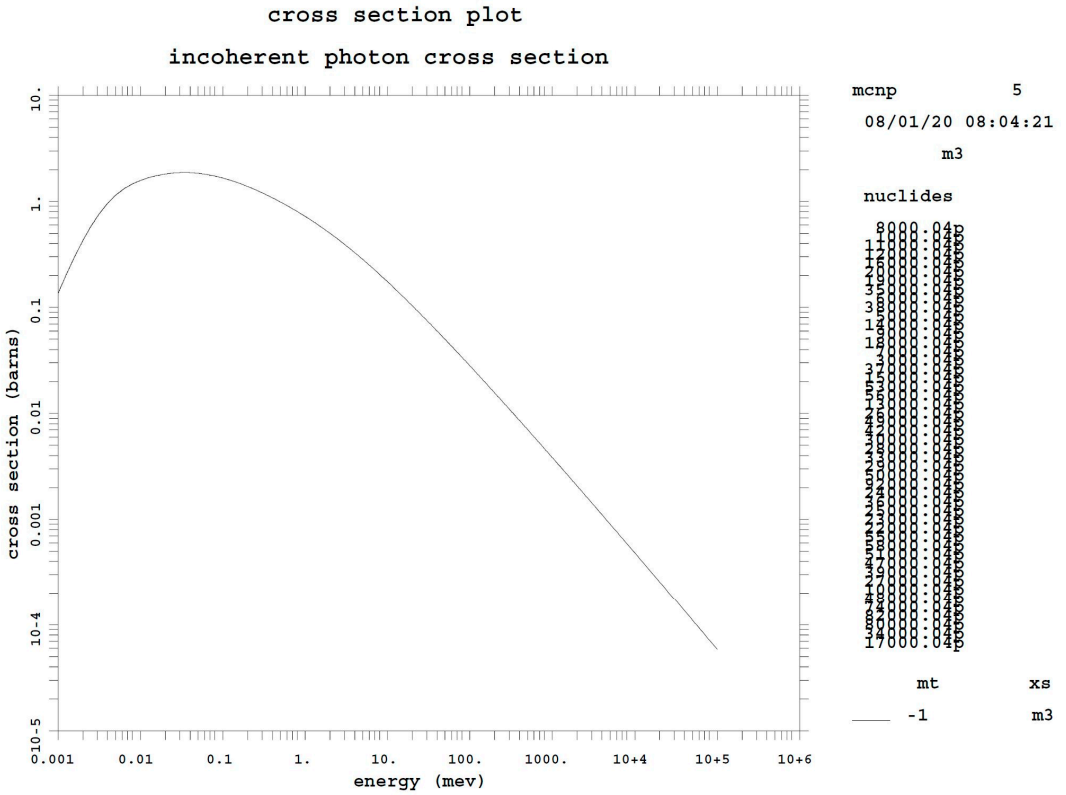

Figure 22. Ocean water incoherent photon cross section as a function of energy.

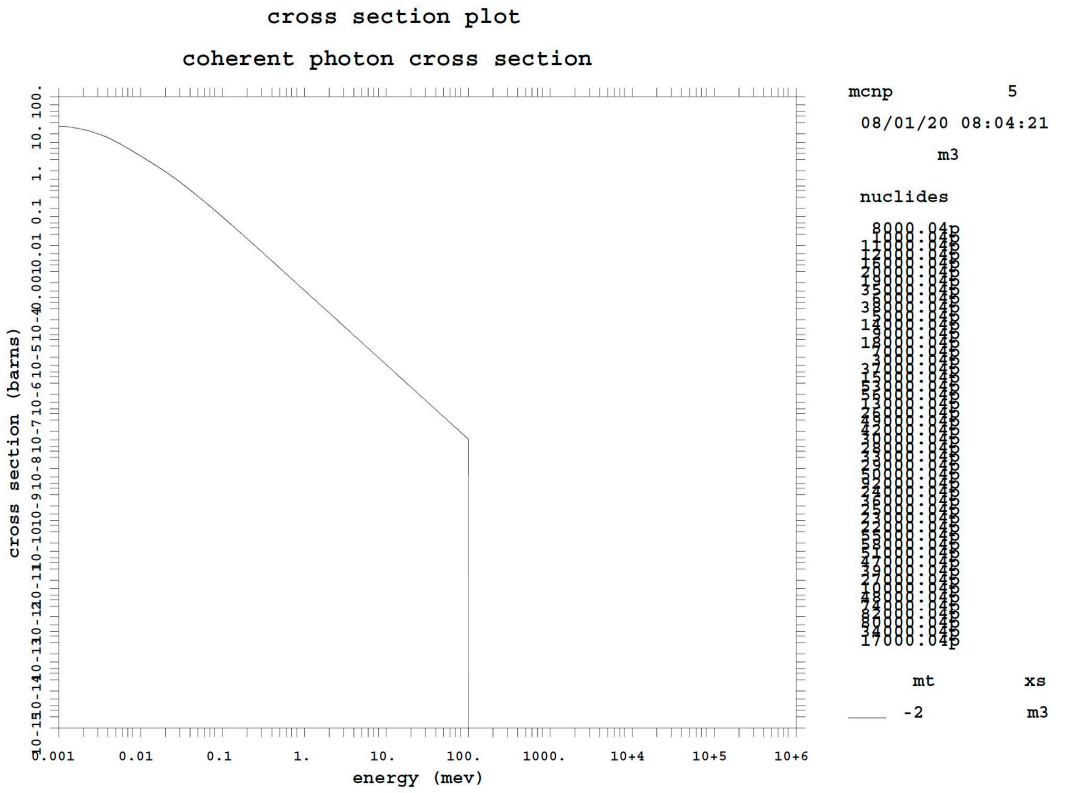

Figure 23. Ocean water coherent photon cross section as a function of energy.

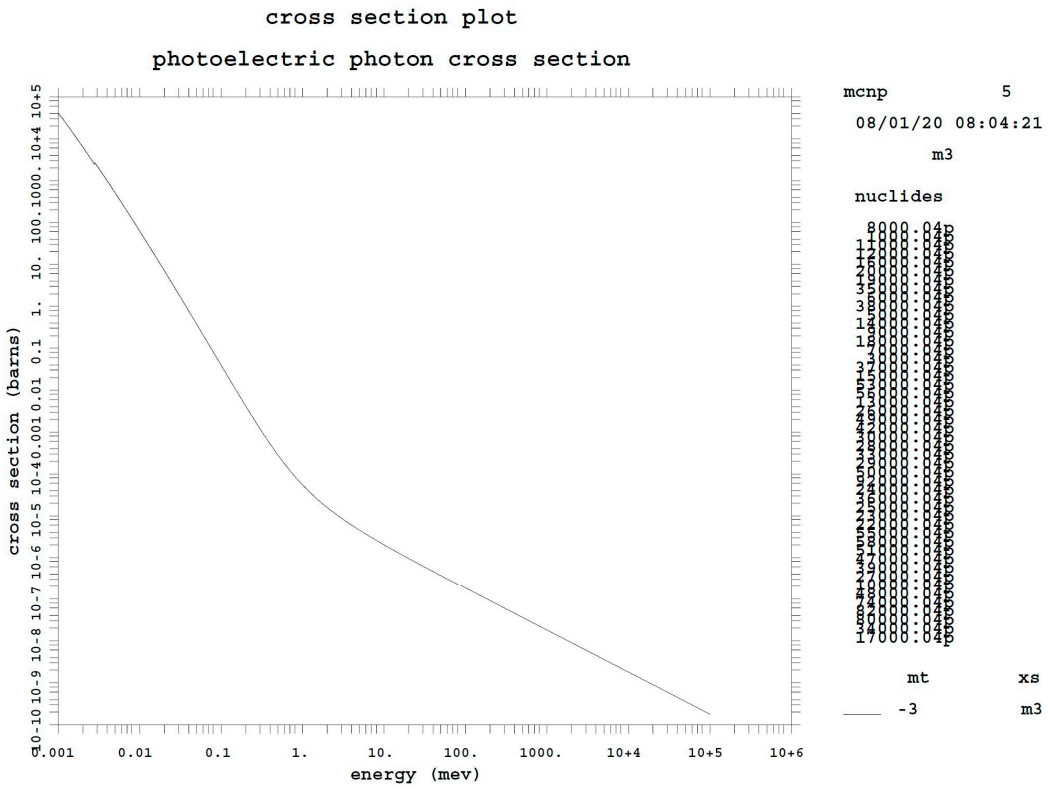

Figure 24. Ocean water photoelectric photon cross section as a function of energy.

3. Results

This section presents the results of the analysis showing the photon fluxes and energy spectra of the Monte Carlo simulations in the presence of polyethylene contaminations and also without it in the detector chamber, located at x = 10 cm on the top of the sample tank on the x-axis.

The study analyzed the photon fluxes and their contributions on three discrete energy bins: 30, 40, and 50 keV at different polyethylene grades with an energy spectrum peak located at 40 keV. The reason of a 40 keV peak can be explained by the cross section considerations and energy spectrum degradation. As shown in Figure 21, the total photon cross section value (in barns) decreases as a function of the energy from 8 barns at 40 keV to 3 barns at 50 keV. Moreover, the detection surface is located at x = 10 cm after the primary injection beam at x = 0 cm, leading to the detection of a particle flux and spectrum in a different energy configuration due to scattering, fluorescence, absorption, and photoelectric effect, which are responsible for leaving an intact high energy photon band after x = 5 cm and thus made negligible the energy contribution for the low band spectrum $E < 20$ keV. Between the interval $5 < x < 10$ cm, the photon flux, present in a high energy band configuration, interacts with the nonhomogeneous media due to scattering, fluorescence, absorption, and photoelectric effect, thus causing a degradation of the 50 keV energy bin and leading to an average value of 40 keV.

As shown in Figures 25 and 26, the total photon flux and each flux that was evaluated on 30, 40, and 50 keV, increase between 0–10 ppm of 1.4% due to electron bremsstrahlung and photelectric-fluorescence on polyethylene particles. However, it has to be underlined that in the beginning of the contamination process, the main atomic element present in the water is oxygen with a weight percentage of 85.70%, and its photon cross sections (Figures 10–14) show a higher value (in barn unities) compared to the carbon ones (Figures 5–9). These cross-section considerations are the main reason to understand the decrease of 5.6% between 10–100 ppm where the amount of oxygen reduces while the amount of carbon increases but with a less effective cross-section value. However, after 100 ppm, due to the electron stopping power and the bremsstrahlung/photoelectric

process on the mixture, the photon flux trend starts to increase 10% up to 1000 ppm and of 50.7% from 1000–10,000 ppm.

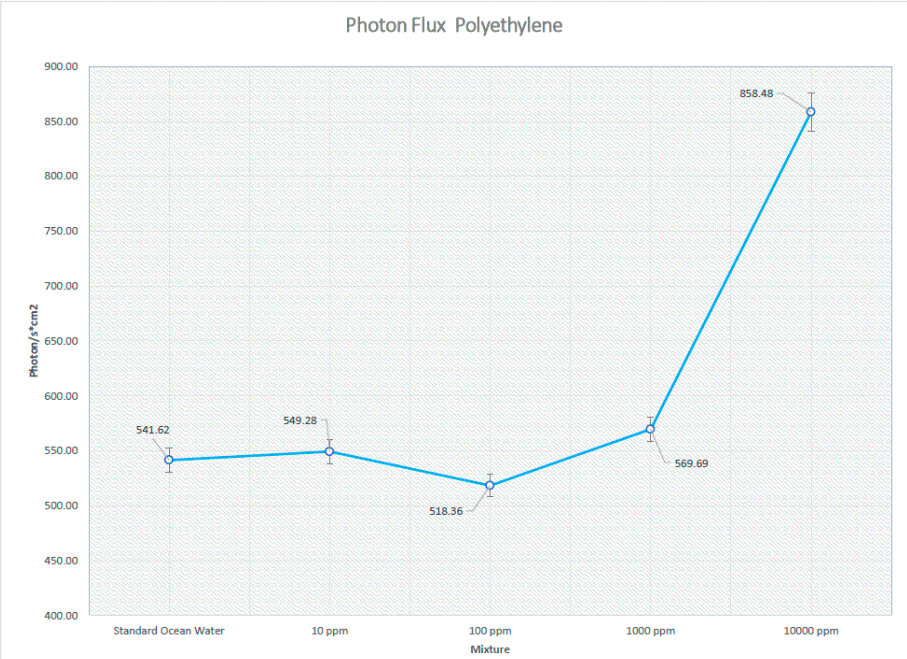

Figure 25. Photon flux—ocean water vs contamination.

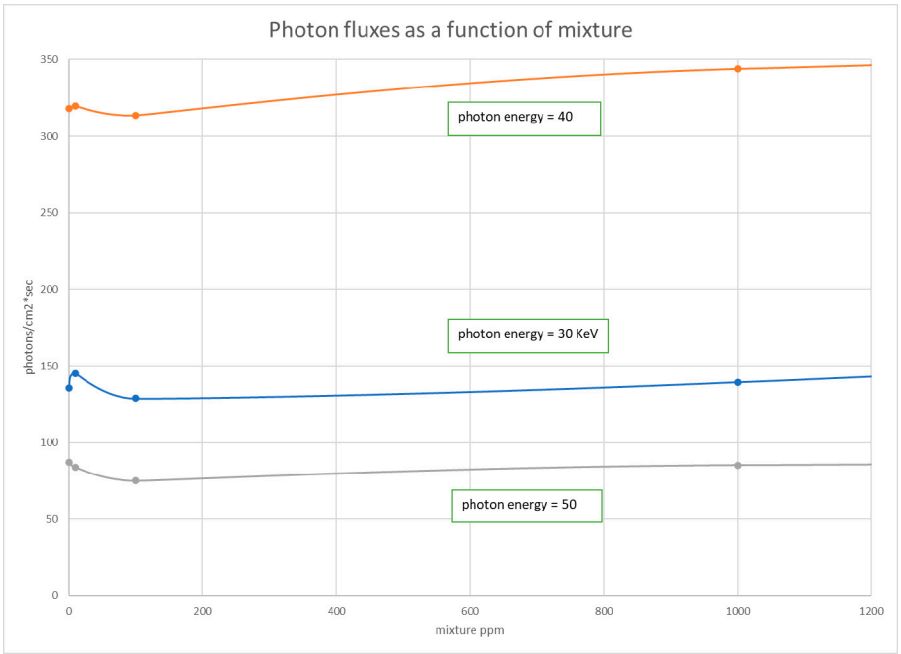

Figure 26. Photon fluxes—spectrum vs contamination.

Figures 25–29 show the fluxes and photon energy spectra and the different behaviors as a function of polyethylene contamination on 3 discrete energy bins.

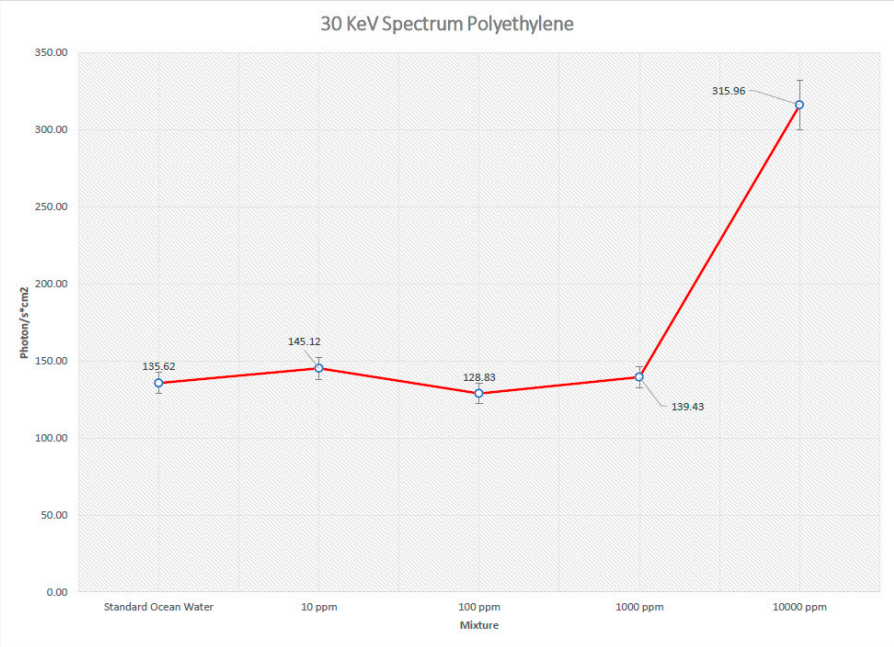

Figure 27. 30 keV—ocean water vs contamination.

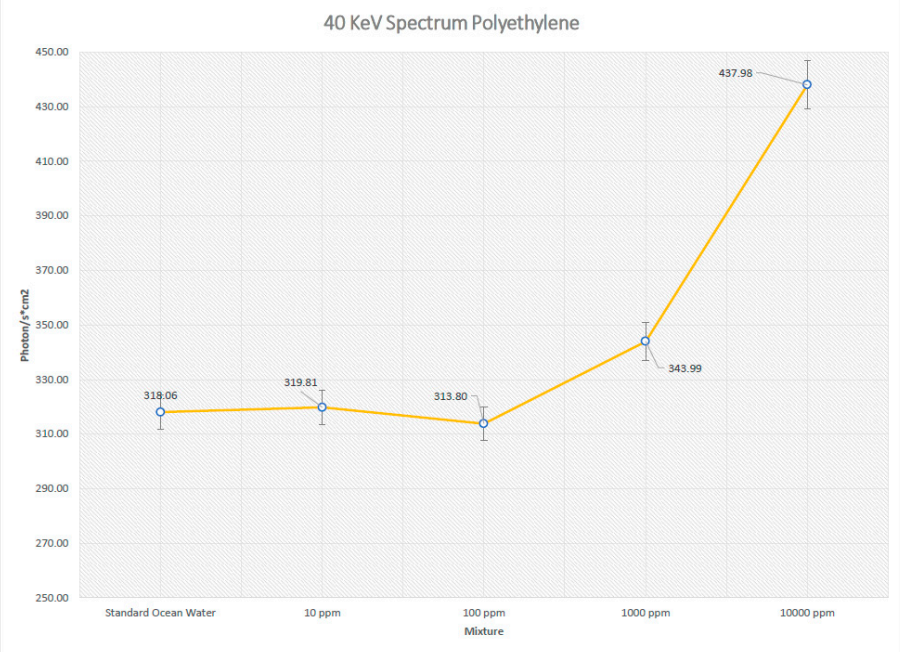

Figure 28. 40 keV—ocean water vs contamination.

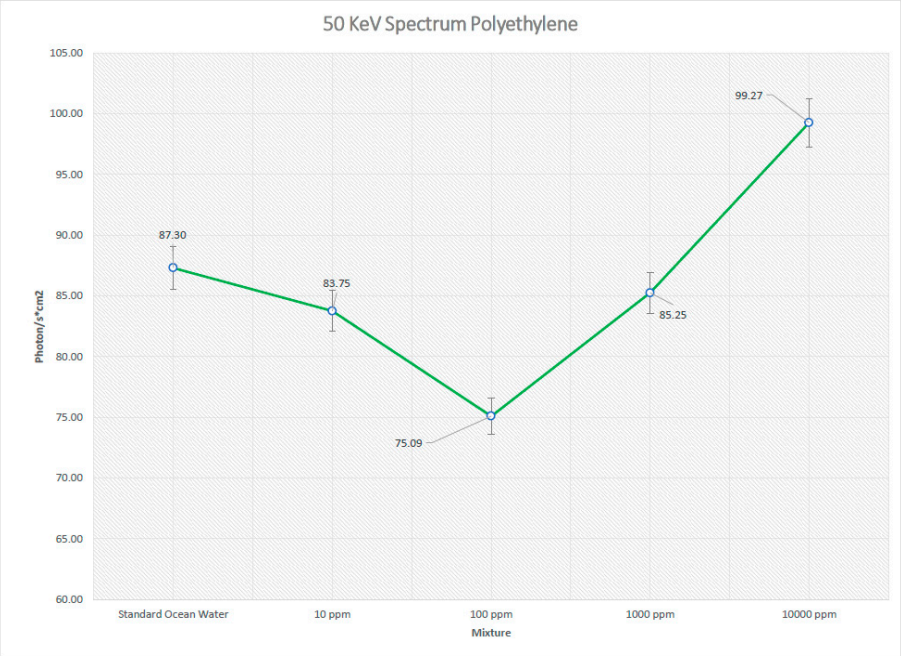

Figure 29. 50 keV—ocean water vs contamination.

As mentioned in Section 2, the graphs in Figures 30–33 show the photon fluxes and energy spectra as well as the different behaviors of fixed contamination test case of 100 ppm polyethylene, in cluster configuration, and mixed as a function of microorganism group PO_4, evaluated on 3 discrete energy bins, i.e., 30, 40, and 50 keV.

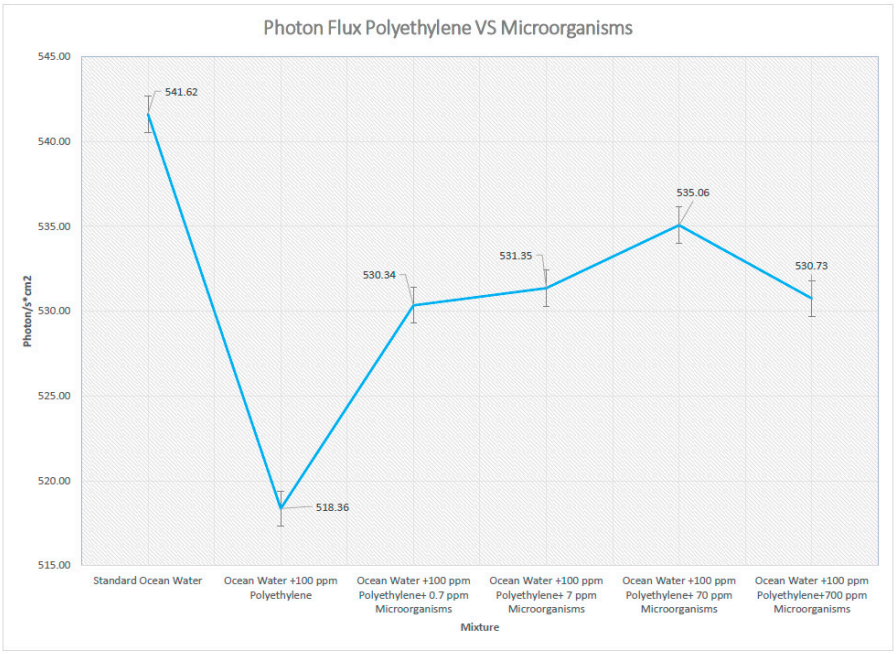

Figure 30. Photon flux—polyethylene vs microorganisms.

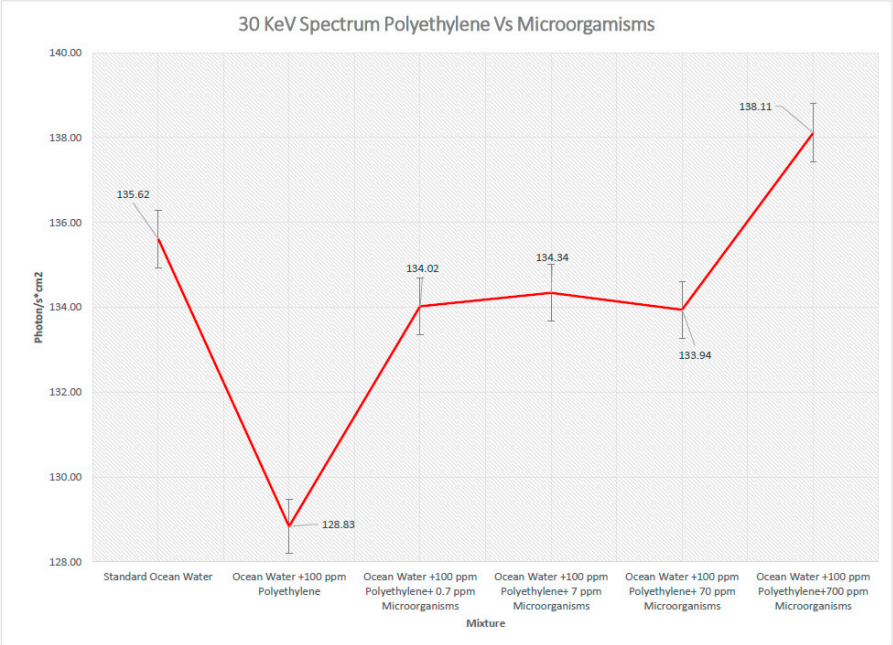

Figure 31. 30 KeV—polyethylene vs microorganisms.

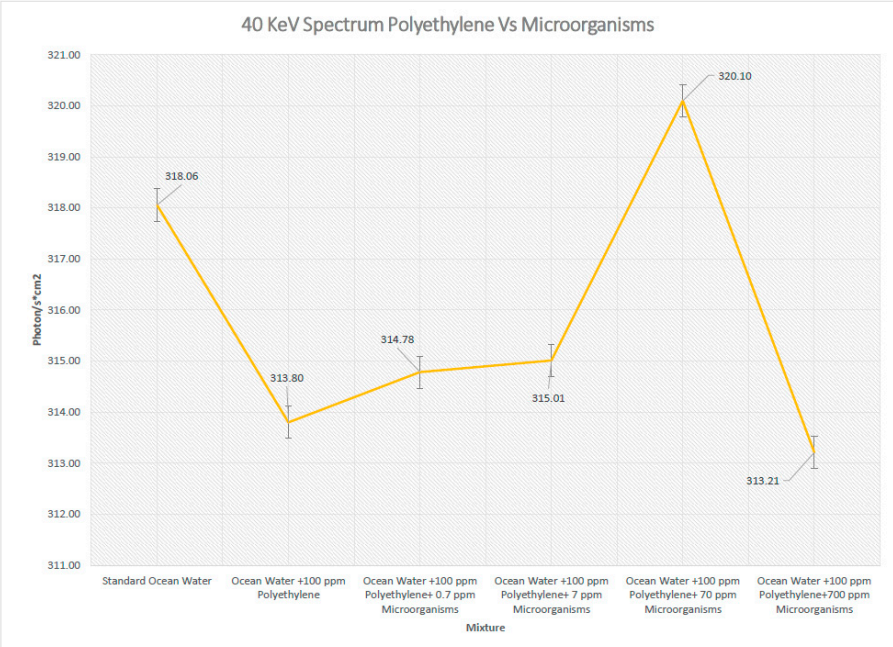

Figure 32. 40 KeV—polyethylene vs microorganisms.

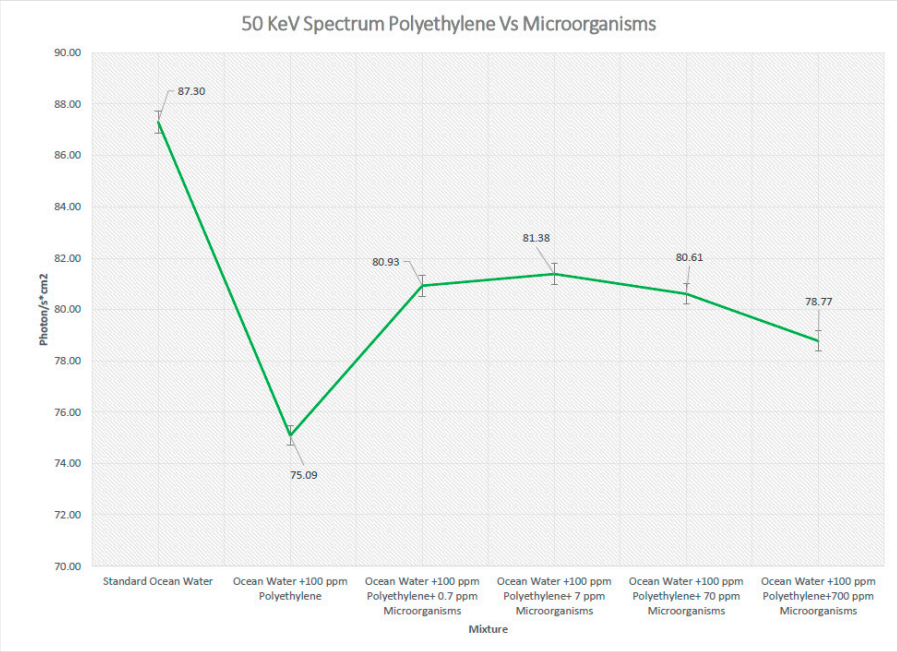

Figure 33. 50 KeV—polyethylene vs microorganisms.

4. Discussion

The photon fluxes and spectra can discriminate the amount of polyethylene contamination by using to its own "particle signature" in terms of photon flux at the detector point combined with the spectrum analysis, as reported for 30, 40, and 50 keV.

As shown in Figures 27–29, the photon flux associated with the sample of ocean water at different concentrations of the polyethylene shows both a trend in term of photon/s*cm^2 and differences from an energy spectrum point of view to evaluate its own contributions in counting the number of photons on each energy line:

1. The 10-ppm polyethylene case can be discriminated using the photon flux counts at the detector evaluated on the 30 and 40 keV spectra compared to the standard ocean water.
2. The 100-ppm polyethylene case can be discriminated using the photon flux counts at the detector and the 30, 40, and 50 keV spectra compared to the 10 ppm one.
3. The 1000-ppm polyethylene case can be discriminated using the photon flux counts at the detector and the 30, 40, and 50 keV spectra compared to the 100 ppm one.
4. The 10,000-ppm polyethylene case can be discriminated using the photon flux counts at the detector and the 30, 40, and 50 keV spectra compared to the 1000 ppm one.

As shown in Figure 30, the photon flux, starting from the ocean water plus 100 ppm polyethylene contamination, increases as a function of the ppm amount of microorganisms added in the water sample tank. This behavior is due to an increase from 0.7 ppm to 700 ppm of P (present in the PO_4 group in the sample) and also due to a change subsequently in the cross-section value, thus affecting the photon population (Figures 15–18). In the presence of microorganism living/nonliving matter, the photon flux shows, taking a parametric comparison case of 100 ppm polyethylene, an increase of 2.3% from 0 to 0.7 ppm of microorganisms, 0.2% from 0.7 to 7 ppm of microorganisms, 0.7% from 7 to 70 ppm of microorganisms, and a decrease of 1% from 70 to 700 ppm of microorganisms. Furthermore, it has to be underlined that even if there is a significant change in the total photon population counts, what has been one of the research main goals was to discriminate the number of microorganisms present in the sample tank through a spectrum analysis and relative photon flux counts on the 3 energy bins.

As shown, the photon flux associated with the 100-ppm polyethylene at different concentrations of microorganisms increases in terms of photon/s*cm^2, and differences appear in the contribution to the total by different energy photons (Figures 31–33):

5. The 0.7-ppm microorganisms case can be discriminated using the photon flux counts at the detector evaluated on the 30 and 50 keV spectrum lines compared to the ocean water + 100 ppm polyethylene combination at the same energy conditions.
6. The 7-ppm microorganisms case can be discriminated using the photon flux counts at the detector evaluated on the 50 keV spectrum line compared to the ocean water + 100 ppm polyethylene + 0.7 ppm microorganisms combination at the same energy condition.
7. The 70-ppm microorganisms case can be discriminated using the photon flux counts at the detector evaluated on the 40 and 50 keV spectrum lines compared to the ocean water + 100 ppm polyethylene + 7 ppm microorganisms combination at the same energy conditions.
8. The 700-ppm microorganisms case can be discriminated using the photon flux counts at the detector evaluated on the 40 and 50 keV spectrum lines compared to the ocean water + 100 ppm polyethylene + 70 ppm microorganisms combination at the same energy conditions.

5. Conclusions

This study proposed a new approach to identify low contaminations of polyethylene mixed in water using a Monte Carlo simulation performed by the MCNPX subatomic particles code and evaluating the secondary photon (generated by an electron beam of 50 keV and 1 μA) energy spectra and fluxes revealed by an adequate detector.

Different types of contamination grades can be discriminated using their trend Vs photon/s*cm^2 evaluated on at least three energy bins, which in this case are 30, 40, and 50 keV. Every single contamination is unique in its own spectrum photon signature, and the flux acts as a unique identifier in the detection process so that, in combination with the microorganisms analysis, it can give the ppm amount of polyethylene in ocean water, drinking/non-drinking water, and food/beverage processing.

Author Contributions: Conceptualization, L.J.T. and P.N.; methodology, L.J.T., P.N. and J.I.A.; software, L.J.T., P.N.; validation, E.M. and J.I.A.; investigation, E.M., D.C.; data curation, R.S.; writing—original draft preparation, P.N., D.C.; writing—review and editing, L.J.T., P.N., J.I.A.; visualization, R.S.; All authors have read and agreed to the published version of the manuscript.

Funding: This research received no external funding.

Acknowledgments: We deeply thank: Giulio Magrin, Alessandro Alemberti, Ilaria A. Valli.

Conflicts of Interest: The authors declare no conflict of interest.

References

1. Parker, L. Microplastics. National Geographic Society. Available online: https://www.nationalgeographic.com/environment/2019/06/microplastics-spread-throughout-deep-sea-monterey-canyon/ (accessed on 20 October 2020).
2. Rogers, K. Microplastics "Plastic Particulate". Britannica. Available online: https://www.britannica.com/technology/microplastic (accessed on 20 October 2020).
3. Kane, I.A.; Clare, M.A.; Miramontes, E.; Wogelius, R.; Rothwell, J.J.; Garreau, P.; Pohl, F. Seafloor microplastic hotspots controlled by deep-sea circulation. *Science* **2020**, *368*, 1140–1145. [CrossRef] [PubMed]
4. Smith, M.; Love, D.C.; Rochman, C.M.; Neff, R.A. Microplastics in Seafood and the Implications for Human Health. *Curr. Environ. Health Rep.* **2018**, *5*, 375–386. [CrossRef] [PubMed]
5. National Research Council (US) Safe Drinking Water Committee. *Drinking Water and Health*; National Academies Press: Washington, DC, USA, 1977.

6. Wesch, C.; Barthel, A.-K.; Braun, U.; Klein, R.; Paulus, M. No microplastics in benthic eelpout (Zoarces viviparus): An urgent need for spectroscopic analyses in microplastic detection. *Environ. Res.* **2016**, *148*, 36–38. [CrossRef] [PubMed]
7. Prata, J.C.; Da Costa, J.P.; Duarte, A.C.; Rocha-Santos, T. Methods for sampling and detection of microplastics in water and sediment: A critical review. *TrAC Trends Anal. Chem.* **2019**, *110*, 150–159. [CrossRef]
8. Maes, T.; Jessop, R.; Wellner, N.; Haupt, K.; Mayes, A.G. A rapid-screening approach to detect and quantify microplastics based on fluorescent tagging with Nile Red. *Sci. Rep.* **2017**, *7*, srep44501. [CrossRef] [PubMed]
9. Araujo, C.F.; Nolasco, M.M.; Ribeiro, A.M.; Ribeiro-Claro, P.J. Identification of microplastics using Raman spectroscopy: Latest developments and future prospects. *Water Res.* **2018**, *142*, 426–440. [CrossRef] [PubMed]
10. Marine & Environmental Research Institute. Guide to Microplastic Identification. 2012. Available online: https://docplayer.net/27438419-Guide-to-microplastic-identification.html (accessed on 20 October 2020).
11. Segebade, C.; Starovoitova, V.N.; Borgwardt, T.; Wells, D. *Principles, Methodologies, and Applications of Photon Activation Analysis: A Review*; Springer: Berlin/Heidelberg, Germany, 2017.
12. Joseph, A.; Cotruvo, W.H.O. *Water, Sanitation and Health Protection and the Human Environment World*; WHO: Geneva, Switzerland, 2006.
13. Fries, E.; Dekiff, J.H.; Willmeyer, J.; Nuelle, M.T.; Ebert, M.; Remy, D. Identification of polymer types and additives in marine microplastic particles using pyrolysis-GC/MS and scanning electron microscopy. *Environ. Sci. Process. Impacts* **2013**, *15*, 1949–1956. [CrossRef]
14. Bar-On, Y.M.; Phillips, R.; Milo, R. The biomass distribution on Earth. *Proc. Natl. Acad. Sci. USA* **2018**, *115*, 6506–6511. [CrossRef]
15. Mann, N.H. The Third Age of Phage. *PLoS Biol.* **2005**, *3*, 753–755. [CrossRef]
16. Wommack, K.E.; Colwell, R.R. Virioplankton: Viruses in Aquatic Ecosystems. *Microbiol. Mol. Biol. Rev.* **2000**, *64*, 69–114. [CrossRef]
17. Suttle, C.A. Viruses in the sea. *Nat. Cell Biol.* **2005**, *437*, 356–361. [CrossRef]
18. Bergh, O.; Børsheim, K.Y.; Bratbak, G.; Heldal, M. High abundance of viruses found in aquatic environments. *Nat. Cell Biol.* **1989**, *340*, 467–468. [CrossRef]
19. Wigington, C.H.; Sonderegger, D.; Brussaard, C.P.D.; Buchan, A.; Finke, J.F.; Fuhrman, J.A.; Lennon, J.T.; Middelboe, M.; Suttle, C.A.; Stock, C.; et al. Re-examination of the relationship between marine virus and microbial cell abundances. *Nat. Microbiol.* **2016**, *1*, 15024. [CrossRef] [PubMed]
20. Brum, J.R.; O Schenck, R.; Sullivan, M.B. Global morphological analysis of marine viruses shows minimal regional variation and dominance of non-tailed viruses. *ISME J.* **2013**, *7*, 1738–1751. [CrossRef]
21. Krupovič, M.; Bamford, D.H. Putative prophages related to lytic tailless marine dsDNA phage PM2 are widespread in the genomes of aquatic bacteria. *BMC Genom.* **2007**, *8*, 236. [CrossRef]
22. Xue, H.; Xu, Y.; Boucher, Y.F.; Polz, M.F. High Frequency of a Novel Filamentous Phage, VCYϕ, within an Environmental Vibrio cholerae Population. *Appl. Environ. Microbiol.* **2011**, *78*, 28–33. [CrossRef]
23. Roux, S.; Krupovic, M.; Poulet, A.; Debroas, D.; Enault, F. Evolution and Diversity of the Microviridae Viral Family through a Collection of 81 New Complete Genomes Assembled from Virome Reads. *PLoS ONE* **2012**, *7*, e40418. [CrossRef]
24. Lawrence, C.M.; Menon, S.; Eilers, B.J.; Bothner, B.; Khayat, R.; Douglas, T.; Young, M.J. Structural and Functional Studies of Archaeal Viruses. *J. Biol. Chem.* **2009**, *284*, 12599–12603. [CrossRef]
25. Prangishvili, D.; Forterre, P.; Garrett, R.A. Viruses of the Archaea: A unifying view. *Nat. Rev. Microbiol.* **2006**, *4*, 837–848. [CrossRef]
26. Mainardi, E.; Donahue, R.J.; Wilson, W.E.; Blakely, E.A. Comparison of microdosimetric simulations using PENELOPE and PITS for a 25 keV electron microbeam in water. *Radiat. Res.* **2004**, *162*, 326–331. [CrossRef]
27. Vilhena, M.D.P.S.P.; Da Costa, M.L.; Berrêdo, J.F.; Paiva, R.S.; Almeida, P.D. Chemical composition of phytoplankton from the estuaries of Eastern Amazonia. *Acta Amaz.* **2014**, *44*, 513–526. [CrossRef]
28. Romera-Castillo, C.; Pinto, M.; Langer, T.M.; Álvarez-Salgado, X.A.; Herndl, G.J. Dissolved organic carbon leaching from plastics stimulates microbial activity in the ocean. *Nat. Commun.* **2018**, *9*, 1–7. [CrossRef]
29. Gin, K.Y.-H.; Lin, X.; Zhang, S. Dynamics and size structure of phytoplankton in the coastal waters of Singapore. *J. Plankton Res.* **2000**, *22*, 1465–1484. [CrossRef]
30. Pelowitz, D.B. *MCNPX User's Manual, Version 2.5.0*; Report LA-CP-05-0369; Los Alamos National laboratory: Los Alamos, NM, USA, 2005.

31. White, M.C. *Photo Atomic Data Library, MCPLIB04*; Los Alamos National Laboratory: Los Alamos, NM, USA, 2003.
32. Oak Ridge National Laboratory. *MCNP-MCNPX Code Collection*; Los Alamos national Laboratory: Los Alamos, NM, USA, 2006.